PCCP

Locking water molecules via ternary O-H···O intramolecular hydrogen bonds in perhydroxylated closo-dodecaborate†

Journal:	*Physical Chemistry Chemical Physics*
Manuscript ID	CP-ART-07-2023-003555.R1
Article Type:	Paper
Date Submitted by the Author:	21-Aug-2023
Complete List of Authors:	Jiang, Yanrong; ShanghaiTech University, Center for Transformative Science Hu, Zhubin; East China Normal University, State Key Laboratory of Precision Spectroscopy Zhong, Cheng; Wuhan University, College of Chemistry & Molecular Sciences Yang, Yan; East China Normal University, State Key Laboratory of Precision Spectroscopy Wang, Xue-Bin; Pacific Northwest National Laboratory, Physical Sciences Division Sun, Zhenrong; East China Normal University, State Key Laboratory of Precision Spectroscopy Sun, Haitao; East China Normal University, State Key Laboratory of Precision Spectroscopy Liu, Zhi; ShanghaiTech University, Center for Transformative Science Peng, Peng; ShanghaiTech University, Center for Transformative Science

ARTICLE

Locking water molecules via ternary O-H···O intramolecular hydrogen bonds in perhydroxylated closo-dodecaborate†

Received 00th January 20xx,
Accepted 00th January 20xx

DOI: 10.1039/x0xx00000x

Yanrong Jiang,[a,b] Zhubin Hu,[b] Cheng Zhong,[d] Yan Yang,[b] Xue-Bin Wang,[c] Zhenrong Sun,[b] Haitao Sun,[*b] Zhi Liu[*a] and Peng Peng[*a]

A multitude of applications around perhydroxylated closo-dodecaborate $B_{12}(OH)_{12}^{2-}$ in condensed phase is inseparable from the fundamental mechanisms underlying high water orientation selectivity based on $B_{12}(OH)_{12}^{2-}$ base. Herein, we directly compare the structural evolution of water clusters, ranging from monomer to hexamer, oriented by functional groups in $B_{12}H_{12}^{2-}$, $B_{12}H_{11}OH^{2-}$ and $B_{12}(OH)_{12}^{2-}$ bases using multiple theoretical methods. A significant revelation is made regarding $B_{12}(OH)_{12}^{2-}$: each additional water molecule is locked into the intramolecular hydrogen bond B-O-H ternary ring in an embedded form. This new pattern of water cluster growth suggests that B-(H-O)···H-O interactions prevail over the competition from water-hydrogen bonds (O···H-O), distinguishing it from the behavior observed in $B_{12}H_{12}^{2-}$ and $B_{12}H_{11}OH^{2-}$ bases, where the competition arises from a mixed competing model involving dihydrogen bond (B-H···H-O), conventional hydrogen bond (B-(H-O)···H-O) and water hydrogen bond (O···H-O). Through aqueous solvation and ab initio molecular dynamics analysis, we further demonstrate the largest water clusters in the first hydrated shell with exceptional thermodynamic stability around $B_{12}(OH)_{12}^{2-}$. These findings provide a solid scientific foundation for the design of boron cluster chemistry incorporating hydroxyl group-modified borate salts with potential implications for various applications.

1. Introduction

As an important non-covalent interaction, inter- and intra- molecular hydrogen bonds (HB) are essential in both natural and artificial structures, ranging from biomacromolecules to supramolecular materials.[1-3] Especially, anionic HB are noteworthy as they are reinforced by strong electric fields.[4-9] This unique property endows them with exceptional capabilities in diverse areas, including aggregation-induced emission enhancement system,[10] novel supramolecular anion cages,[11] and transmembrane anion transport.[12] However, anionic HB is highly susceptible to the environmental interference due to the competition between ion-water interactions and inter-water HB in aqueous solutions. These subtle competition mechanisms highlight the effects of anionic HB, which is an eternal topic due to its essential role in surface and interface chemistry,[13-17] electron-driven chemistry,[18, 19] mass transfer kinetics[20] and solvation sheath structure.[21] Several major open questions regarding anionic HB have been extensively investigated for smaller-sized anions,[6, 22-28] including the binding motif of the electron or energy extrapolation from water clusters to bulk water, the competitive mechanism of HB, the characteristics of the local first solvation shell, and the thermally activated behaviour under the latent asymmetry of electron density of hydrated anionic clusters. Recently, there is a growing demand to expand the exploration to encompass larger functional anions with specific electronic structures and charge distributions. Therefore, it is necessary to build a reasonable model and reveal the influence of these anionic HB on the solvation process.

Our attention has been drawn to an icosahedral borane dianion, closo-$B_{12}H_{12}^{2-}$, which contains electron-deficient three-center two-electron (3c2e) bonds and an excess of delocalized σ-electron density with two negative charges.[29-31] Moreover, the negatively charged hydrogen in B-H bond can form hydric-to-protonic $X–H^{\delta+}\cdots H^{\delta-}–B$ dihydrogen bond (DHB).[32, 33] These distinctive properties have been extensively studied[34] and have found applications in diverse fields, including indirect hydrogen storage material,[35] boron neutron capture therapy (BNCT) agents or pharmacophores,[36] and enzyme inhibitors.[37, 38] In general, these macroscopic behaviors under condensed phase are intimately linked to the microscopic solvation mechanism governed by anionic HB and intra water-HB. In our previous work,[32] we established an ideal model, $B_{12}H_{12}^{2-}\cdot H_2O$, to explore these phenomena. Our findings revealed that the $O–H^{\delta+}\cdots H^{\delta-}B$ dihydrogen bond is stronger than the $O–H^{\delta+}\cdots X^{-}B$ conventional HB of $B_{12}X_{12}^{2-}\cdot H_2O$ (X = F, I).[32] To connect the molecular-level information with the macroscopic behavior, we further investigated the microhydrated borane clusters $B_{12}X_{12}^{2-}\cdot nH_2O$ (n = 1-6) to gain a deeper understanding of the collective cooperativity of anionic HB and intra water-HB.[39] The results show that highly structured water networks are weaved by joint DHB and water-HB interaction in hydrated $B_{12}H_{12}^{2-}$ cluster. Moreover, we were intrigued by the modification effect of B-H bond, especially the selective

[a] Center for Transformative Science, ShanghaiTech University, Shanghai 201210, China. Email: pengpeng@shanghaitech.edu.cn, liuzhi@shanghaitech.edu.cn
[b] State Key Laboratory of Precision Spectroscopy, East China Normal University, Shanghai 200241, China. Email: htsun@phy.ecnu.edu.cn
[c] Physical Sciences Division, Pacific Northwest National Laboratory, 902 Battelle Boulevard, P.O. Box 999, Richland, Washington 99352, USA
[d] College of Chemistry & Molecular Sciences, Wuhan University, Wuhan Hubei 430072, China

†Electronic Supplementary Information (ESI) available: see attached text for supporting information

functionalization of the B-H to B-O-H vertices achieved by two efficient pathways, i.e., acid-catalyzed reaction[40, 41] and oxidation with hydrogen peroxide.[42-44] The per-hydroxylated closo-dodecaborate $B_{12}(OH)_{12}^{2-}$ bearing twelve organic linkers have intriguing properties that find applications in various fields, e.g., molecular cross-linking skeleton,[45] electrolyte materials,[46] coordination polymers,[47] and MRI contrast agents.[48] Despite its fundamental role in multitudinous research areas, the intrinsic electronic structure and related anionic HB in micro-solvation still need to be investigated.

In this work, we conducted comprehensive theoretical investigations on mono- and per-hydroxylated dodecaborate ($B_{12}H_{11}OH^{2-}$, $B_{12}(OH)_{12}^{2-}$) to gain a deeper understanding of their electronical stability, the structural arrangements in solvation processes and corresponding thermodynamic stability. The four closed ternary O-H intramolecular hydrogen bonds of $B_{12}(OH)_{12}^{2-}$ give full play to its unique function in the layout of water clusters, ignoring the external competition from intra-water HB. Each water molecule falls inside the claw formed by the ternary O-H bonds associated with the strong anionic HB, as revealed by the SAPT2+[49, 50]/aug-cc-pVTZ method. This behaviour differs from the hydration pathway observed in $B_{12}H_{11}OH^{2-}$, where a combination of DHB, water HB, and conventional HB formed by a single B–OH vertex is involved. Additionally, the modification of B-H vertices to B-OH in $B_{12}(OH)_{12}^{2-}$ leads to larger water shell with improved thermal stability. This modification likely alters the electronic and steric properties of the compound, enhancing its interaction with water molecules and making it more stable under different conditions.

2. Computational methods

A well-designed conformation search strategy with gradient accuracy is comprehensively applied to obtain the global minimum and low-lying isomers of $B_{12}H_{12-m}(OH)_m^{2-}{\cdot}nH_2O$ (m = 1, 12; n = 1−6). Combined with semi-empirical method, the sample of initial guess conformations can reach millions by iterative cyclic accumulation incorporated with a homemade automatic judgment convergence rule. The initial optimization screening was performed by semi-empirical method of GFN2-xTB based on Molclus code. [51-53] A medium precision single point calculation and optimization procedure are then performed to sort the isomers using r2SCAN-3c method embedded in ORCA 5.0.3 codes.[54] Further energy-based structural screening is efficiently conducted at the ωB97X-2/ma-def2-TZVP level with Grimme's dispersion corrections[55, 56] and re-optimized at the PBE0/aug-cc-pVTZ[57, 58] level. The final energy level is set to the 20K Gibbs free energy, which consists of electronic energy at the DLPNO-CCSD(T)[59, 60]/aug-cc-pVTZ level using ORCA code and thermal correction energy at the PBE0/aug-cc-pVTZ level to ensure the most stable structure and related isomers without imaginary frequencies. The scaling factor for zero-point energy were set as 0.9771.[61] The vertical detachment energies (VDEs) calculated at the PBE0/aug-cc-pVTZ level was obtained by the energy differences between the corresponding monoanions and dianions based on the dianions' optimized geometries. And the IP-EOM-DLPNO-CCSD method[62] with aug-cc-pVTZ basis set have been verified to predict ionization potential values with good accuracy in our previous results, which is also applied in this work. Based on the most stable structures of $B_{12}H_{12-m}(OH)_m^{2-}{\cdot}nH_2O$ (m = 1, 12; n = 1−6), the energy decomposition analysis of weak interaction between borane monomer and remaining water shell was performed at the SAPT2+[49, 50]/aug-cc-pVDZ level employing two-body symmetry adapted perturbation theory (SAPT) using PSI4 code.[63] The plots of independent gradient model based on Hirshfeld partition (IGMH) were generated by the Multiwfn code[64] and rendered by the VMD program.[65] All DFT calculations were carried out using the Gaussian 16 software.[66] Ab initio molecular dynamics (AIMD) simulations were performed using the ORCA code. And the force-field molecular dynamics simulations and analyses of trajectories were conducted using the GROMACS code.[67] (see details in the *Supporting Information*, SI)

3. Results and discussion

3.1 Hydroxylation mechanism of $B_{12}H_{12}^{2-}$

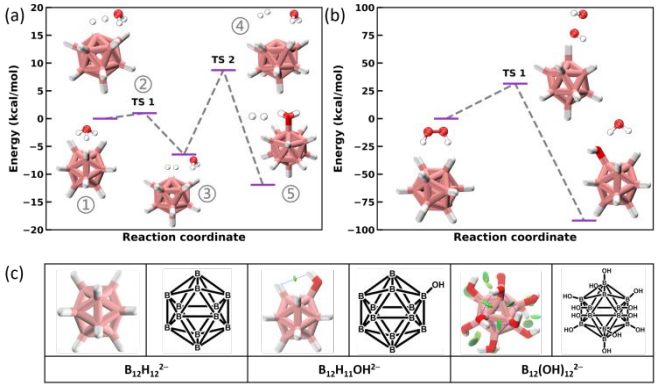

Fig. 1. Reaction mechanisms and energy profiles of $B_{12}H_{12}^{2-}$ mono-hydroxylation (a) catalyzed by H_3O^+ under aqueous sulfuric acid and (b) oxidated by hydrogen peroxide calculated at the DLPNO-CCSD(T)/aug-cc-pVTZ level. (c) Two- and three-dimensional schematic diagrams and plots of the independent gradient model based on Hirshfeld partition (IGMH) of $B_{12}H_{12-m}(OH)_m^{2-}$ (m = 0, 1, 12). The intramolecular hydrogen bonds are indicated by the blue dashed line. Blue, green, and red isosurface represents the strong electrostatic interaction, the weak van der Waals interaction, and the strong repulsive interaction, respectively (isovalue = 0.05). The ball-stick models with B, H, and O atoms are in pink, white, and red, respectively.

The hydroxylation of $B_{12}H_{12}^{2-}$ was previously mainly carried out using two protocols: sulfuric acid and hydrogen peroxide. Both protocols resulted in the formation of $B_{12}(OH)_{12}^{2-}$. Our results revealed two distinct reaction pathways: a two-step route catalyzed by H_3O^+ under aqueous sulfuric acid[40, 41] (Fig. 1a) and a one-step oxidation by hydrogen peroxide[42] (Fig. 1b), respectively. The energy barrier was calculated at the DLPNO-CCSD(T) /aug-cc-pVTZ level, for sulfuric acid catalysis reaction with 8.7 kcal/mol and hydrogen peroxide oxidation reaction with 31.5 kcal/mol. The intrinsic reaction paths and energy profiles of the transition states in two reactions were shown in Fig. S1. Consequently, we observed that the hydrogen atoms in H_3O^+ and H_2O_2 were directed towards the H atoms in polyhedral $B_{12}H_{12}^{2-}$, resulting in strong dihydrogen bonding interactions at the B-H···H-O interfaces. The dehydrogenation process in the former pathway may involve nuclear quantum effect,[68] which hold significant implications for the advancement of green propellant and hydrogen storage

technology. While in latter reaction, the isolated oxygen atom in H_2O_2 attacks the relatively positively charged B atom and links to the H of the B-H vertex to form the B-O-H hydroxyl.

The discovery of B-H polyfunctional hydroxylation reaction led to a variety of polyhedral structures, such as $B_{12}H_{10}(OH)_2^{2-}$ and $B_{12}H_9(OH)_3^{2-}$ and eventually progressively evolved into the 12-fold hydroxylated derivatives $B_{12}(OH)_{12}^{2-}$ with C_3 symmetry, which has not been previously emphasized. Intrigued by the relatively high symmetry of $B_{12}(OH)_{12}^{2-}$, we conducted a weak interaction analysis using the independent gradient model based on Hirshfeld partition (IGMH). In contrast to the previously reported intermolecular dihydrogen bonding involving the 12 B-H vertices in $B_{12}H_{12}^{2-}$, the mono B-O-H bonds in $B_{12}H_{11}OH^{2-}$ exhibits the distinct characteristic of intramolecular dihydrogen bonding with a green interaction zone, as shown in Fig. 1c. Interestingly, four identical closed ternary O-H···O bonds were observed in $B_{12}(OH)_{12}^{2-}$ with 12 green action zones. This internal interfacing would potentially engender unique properties not typically observed in boron-rich materials.

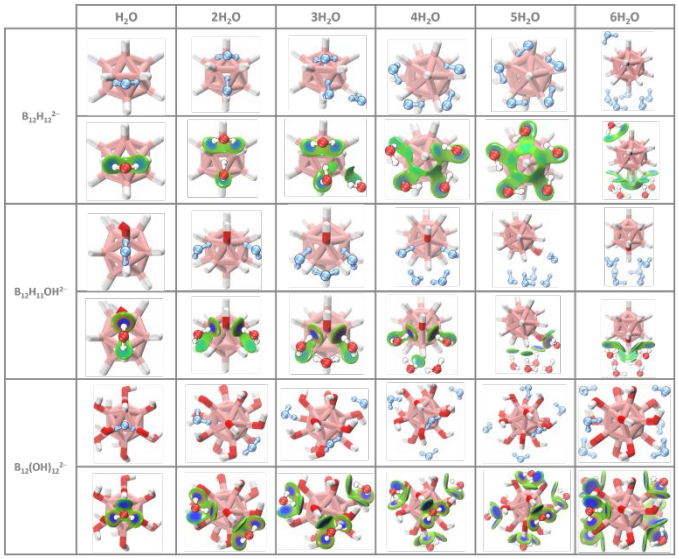

Fig. 2. Structural evolution of monomer to hexamer micro-hydrating cage and corresponding IGMH plots based on B-H···H-O DHBs, B-H···H-O/B-O-H···O-H mixed di-traditional HBs, and ternary B-O-H···O-H HBs in $B_{12}H_{12-m}(OH)_m^{2-}{\cdot}nH_2O$ (m = 0, 1, 12; n = 1−6), respectively. The water molecules were shown in light blue for pure hydrated hydroxylation structures.

3.2 Structural arrangement in solvation process

Benefiting from an ideal model $B_{12}X_{12}^{2-}{\cdot}H_2O$ (X = H, F, I), previous experimental and theoretical results have drawn a consistent conclusion that B-H···H-O DHB is superior to the conventional B-X···H-O HBs (X = F, I), even prevailing over the prototypical strong HB with X = F.[32] And water monomer to hexamer can be arranged with a uniform binding mode in $B_{12}H_{12}^{2-}{\cdot}nH_2O$ due to the subtle competition between B-H···H-O (solute – solvent) and O···H-O (solvent – solvent) water-HBs (Fig. 2).[39] Here, we were curious to know the difference between the DHB system $B_{12}H_{12}^{2-}$ and the corresponding mono- and per- hydroxylated derivatives of $B_{12}H_{11}OH^{2-}$ and $B_{12}(OH)_{12}^{2-}$ regarding hydration shell formation in their immediate vicinity. The most stable topology structures were shown in Fig. 2, while the top three lowest-lying energy conformers were displayed in Fig. S2. To clearly visualize the sites of action of water molecules surrounding the hydroxylated derivatives, an intuitive and semi-quantitative estimation of the intermolecular interaction can be obtained through IGMH analysis. This analysis allows for an examination of various patterns of noncovalent interactions (Fig. 2 and Fig. S3). In the IGMH analysis, the intermolecular interaction can be categorized into three types based on their strength: strong electrostatic attraction (in blue, such as DHB and conventional HB interactions), weak van der Waals interactions (in green, dispersion interaction), and strong repulsions (in red, steric effects).

Fig. 2 shows the mono B-O-H vertex in $B_{12}H_{11}OH^{2-}$ elaborately regulated the water orientation from monomer to hexamer by simultaneously considering the intermolecular DHB system and water hydrogen bond networks. Especially in the case of a small amount of water (n < 4), the arrangement of water molecules is predominantly influenced by the B-O-H vertex due to the significant negative charge present in the single O-H, as illustrated in Fig. S4. This arrangement somewhat resembles the structure of hydrated OH^- as reported by Wang et al..[69] For $B_{12}H_{11}OH^{2-}{\cdot}H_2O$, the two vertices of hydrogen in water are individually connected to B-O-H and B-H, forming a mixed combination of typical B-(H-O)···H-O HB and B-H···H-O DHB. And in the former case, a larger blue region with stronger electrostatic interaction was observed compared to the other endpoint of B-H···H-O DHB. This indicates that when a second water molecule is added, it also attached symmetrically to the B-O-H endpoint, resembling the structure of pure $OH^-{\cdot}2H_2O$. And the remaining two H atoms in both water molecules form B-H···H-O DHB with long interaction distance. For the $B_{12}H_{11}OH^{2-}{\cdot}3H_2O$ cluster, the third water molecule is added without direct contact with $B_{12}H_{11}OH^{2-}$, but it is bonded to the two O atoms of water based on the original $B_{12}H_{11}OH^{2-}{\cdot}2H_2O$ configuration shown in the IGMH plots. This water arrangement is similar to the second lowest-energy isomer of $OH^-{\cdot}3H_2O$, rather than the most stable one, due to the steric requirements of inter-DHB. For n = 4, there's still one water molecule that remains excluded without directly contacting to the base. While as for n = 5, a noncyclic pentamer with three dimensional (3D) topological configurations were formed through the cooperation of the inter-water hydrogen bond and DHB bonds. This configuration is consistent with the second higher-energy isomer of pure $5H_2O$ and $B_{12}H_{12}^{2-}{\cdot}5H_2O$ as reported previously.[70] It is also similar to the prismatic lowest-energy structure of hydrated halogenated $B_{12}X_{12}^{2-}{\cdot}5H_2O$ (X = F, I). For n = 6, the hydroxyl functional group once again shows subtle difference in controlling the water configuration. Two water molecules maintain the water shape observed in $B_{12}H_{11}OH^{2-}{\cdot}2H_2O$, while the remaining four water molecules adopt a flat square form, unlike the sixth water in $B_{12}H_{12}^{2-}{\cdot}6H_2O$.

Upon sequential hydration of $B_{12}H_{11}OH^{2-}$, the mono hydroxyl group have certain effect on the arrangement of solvent layers during the solvation process. Notably, the averaged negative charge of single O-H in 12-fold hydroxylated derivatives $B_{12}(OH)_{12}^{2-}$ with C_3 symmetry approach that in $B_{12}H_{11}OH^{2-}$ (Fig. S4), resulting in more nucleophilic sites and a unique hydrated shell. For $B_{12}(OH)_{12}^{2-}{\cdot}H_2O$ cluster, the water molecule was completely trapped in a cage formed by three B-O-H endpoints with two H atoms attaching O atoms of two B-O-H vertices and one O atom attaching H atom of B-O-H. The

total interaction zone formed by three acting sites resembles a cloverleaf in Fig. 2. Subsequently, each additional water molecule falls into the adjacent closed B-O-H ternary ring without touching other water clusters. Moreover, in the top three lowest-lying isomers, each added water molecule is nested within the negatively charged B-O-H ternary ring with strong grasping force as shown in Fig. S2. Unlike the competition between B-H/(O-H)···H-O (solute-solvent) and O-H···O (solvent-solvent) interactions in hydrated $B_{12}H_{12}^{2-}$ and $B_{12}H_{11}OH^{2-}$ clusters, the closed ternary O-H bonds in $B_{12}(OH)_{12}^{2-}$ effectively locked the H_2O molecules, ignoring the competition of water-hydrogen bonds. With up to $6H_2O$, each B-O-H vertex participates in the locking behavior, forming a 3+3 configuration on both sides with C_2 symmetry.

Table 1. Experimental vertical detachment energies (VDEs) and comparison with calculated VDEs using PBE0 and IP-EOM-DLPNO-CCSD methods with the aug-cc-pVTZ basis set for $B_{12}H_{12-m}(OH)_m^{2-}\cdot nH_2O$ (m = 0, 1, 12; n = 0–6) (in eV).

VDE	$B_{12}H_{12}^{2-a}$			$B_{12}H_{11}OH^{2-}$		$B_{12}(OH)_{12}^{2-}$	
	Expt.	IP-EOM-DLPNO-CCSD	PBE0	IP-EOM-DLPNO-CCSD	PBE0	IP-EOM-DLPNO-CCSD	PBE0
	1.15	1.31	1.29	0.81	0.70	0.58	0.47
1 H_2O	1.46	1.63	1.61	1.27	1.19	0.73	0.60
2 H_2O	1.73	1.90	1.88	1.65	1.59	0.87	0.74
3 H_2O	1.97	2.13	2.11	1.92	1.87	1.04	0.91
4 H_2O	2.19	2.36	2.34	2.19	2.14	1.25	1.13
5 H_2O	2.31	2.49	2.46	2.19	2.13	1.29	1.16
6 H_2O	2.53	2.77	2.75	2.39	2.33	1.53	1.40

[a]The experimental and calculated VDEs of $B_{12}H_{12}^{2-}\cdot nH_2O$ were derived from ref.[32, 39]

3.3 Vertical detachment energies and binding energies

In order to characterize the electron binding energies in hydrated hydroxylated borane, a systematic study was conducted using quantum chemical calculations. It has been previously verified that IP-EOM-DLPNO-CCSD/aug-cc-pVTZ method can qualitatively and quantitatively reproduce the experimental measurements of vertical detachment energy (VDE) for $B_{12}H_{12}^{2-}\cdot nH_2O$ (n = 0–6), as shown in Table 1.[32, 39] Therefore, the same method was applied in this work to ensure reliable results. Fig. 3(a) shows that VDEs of mono- and per-hydroxylated boranes and their corresponding hydrates are lower than that of $B_{12}H_{12}^{2-}\cdot nH_2O$ (n = 0–6). This change in ionization properties can be attributed to the position of the highest occupied molecular orbital (HOMO) and the distribution of excess negative charge (Fig. S4 and S5). Previous investigations on $B_{12}X_{12}^{2-}$ (X = H, F, Cl) have shown that the excess detached electron is usually taken from the most positively charged region of boron core, where the HOMO is mainly located.[31, 71] Compared to an averaged 92% contribution of boron core in $B_{12}H_{12}^{2-}\cdot nH_2O$, the HOMO distributions in $B_{12}H_{11}OH^{2-}\cdot nH_2O$ and $B_{12}(OH)_{12}^{2-}\cdot nH_2O$ gradually shifts to the hydroxyl shell, where the averaged contribution of boron core drops to 79% and 62%, respectively (Fig. S5). Additionally, the hydroxylated groups also carry a higher excess of negative charges (Fig. S4). These factors contribute to the lower VDEs observed in the hydrated hydroxyl clusters compared to $B_{12}H_{12}^{2-}\cdot nH_2O$. It is worth noting that in Fig. 3a, a slight VDE increment of 0.12 eV can be seen from n = 4 to 5 for $B_{12}H_{12}^{2-}\cdot nH_2O$. While $B_{12}H_{11}OH^{2-}\cdot nH_2O$ and $B_{12}(OH)_{12}^{2-}\cdot nH_2O$ exhibit a distinct "plateau" with a VDE shift of only 0.01 eV and 0.04 eV, respectively. This behaviour is similar to the 0.03 eV VDE shift observed in $B_{12}F_{12}^{2-}\cdot nH_2O$ from n = 4 to 5. Subsequently, when n = 6, the VDE of all three hydrates continues to increase.

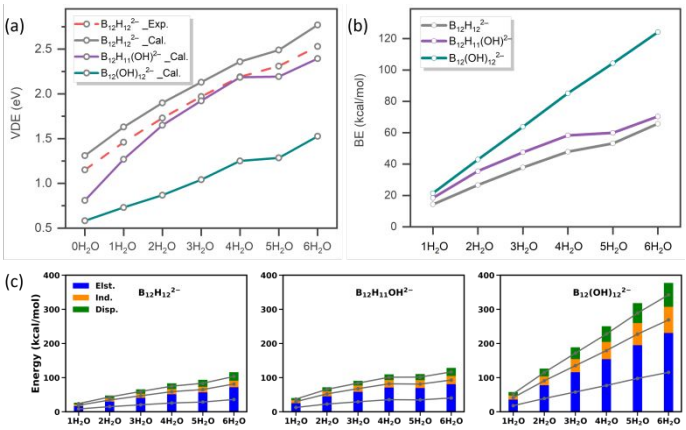

FIG. 3. (a) Experimental (dashed line) and calculated (solid line) VDEs of $B_{12}H_{12-m}(OH)_m^{2-}\cdot nH_2O$ (m = 0, 1, 12; n = 0–6) at the IP-EOM-DLPNO-CCSD/aug-cc-pVTZ level. (b) Total binding energies (BE, in kcal/mol) for $B_{12}H_{12-m}(OH)_m^{2-}\cdot nH_2O$ (m = 0, 1, 12; n = 1–6) calculated at the SAPT2+/aug-cc-pVDZ level. (c) Electrostatic (Elst., blue), induction (Ind., yellow), and dispersion (Disp., green) attraction terms (kcal/mol) derived from energy decomposition analysis for $B_{12}H_{12-m}(OH)_m^{2-}\cdot nH_2O$ (m = 0, 1, 12; n = 1–6) calculated at the SAPT2+/aug-cc-pVDZ level.

The magnitude and nature of weak interaction in $B_{12}H_{11}OH^{2-}\cdot nH_2O$ and $B_{12}(OH)_{12}^{2-}\cdot nH_2O$ also change upon the addition of water molecules, as shown in Fig. 3(b, c) and Table S2. For mono hydrate of $B_{12}H_{11}OH^{2-}$ and $B_{12}(OH)_{12}^{2-}$ bases, the total binding energies (BE) are 4.07 and 7.14 kcal/mol higher than that of $B_{12}H_{12}^{2-}\cdot H_2O$, which is consistent with the simulated infrared spectrum (Fig. S6). The strong binding energy in $B_{12}(OH)_{12}^{2-}\cdot H_2O$ leads to the largest blue shift of 46 cm^{-1} in typical bend vibrational modes in H_2O, compared to the shifts of 34.4 and 0.9 cm^{-1} observed in $B_{12}H_{11}OH^{2-}\cdot H_2O$ and $B_{12}H_{12}^{2-}\cdot H_2O$, respectively. Normally, the VDE difference between a hydrated anion and the corresponding isolated anion (ΔVDE), defined as $[E(B_{12}H_{12-m}(OH)_m^{2-}\cdot H_2O) - E(B_{12}H_{12-m}(OH)_m^{2-})] - [E(B_{12}H_{12-m}(OH)_m^{\bullet-}\cdot H_2O) - E(B_{12}H_{12-m}(OH)_m^{\bullet-})]$, can be considered as a direct estimate for measuring the binding energy (BE) between the water and anions,[39, 72] However, this ΔVDE predicted BE trend among $B_{12}H_{12-m}(OH)_m^{2-}\cdot H_2O$, i.e., BE (m = 1) > BE (m = 0) > BE (m = 12), contradicts the results of BE (m = 12) > BE (m = 1) > BE (m = 0) revealed by both SAPT2+/aug-cc-pVTZ and SAPT0/jun-cc-pVDZ methods as listed in Table S3. This incorrect prediction can be attributed to the fact that each B-O-H vertex carry uniformly large number of negative charges, so the single charged $B_{12}(OH)_{12}^{\bullet-}$ still maintains a strong binding energy with H_2O molecule calculated at the SAPT0/jun-cc-pVDZ level. While for $B_{12}H_{11}OH^{2-}$, the single OH endpoint involved in HOMO distribution has little effect on the binding energy of $B_{12}H_{11}OH^{\bullet-}\cdot H_2O$. Therefore, the advantage of BE in $B_{12}H_{11}OH^{2-}\cdot H_2O$ over $B_{12}H_{12}^{2-}\cdot H_2O$ can be well reproduced by ΔVDE.

In addition, the BEs maintains an advantage in $B_{12}H_{11}OH^{2-}\cdot nH_2O$ compared to the hydrated $B_{12}H_{12}^{2-}$ cluster. However, this BE advantage decreases at n = 5, and further reduces to 4.65 kcal/mol at n = 6. Note that the linear BE of $B_{12}(OH)_{12}^{2-}\cdot nH_2O$ consistently surpasses the other two clusters, and at n = 6, the BE gap between $B_{12}(OH)_{12}^{2-}\cdot nH_2O$ and $B_{12}H_{12}^{2-}\cdot nH_2O$ reaches an astonishing 51 kcal/mol. This can be ascribed to the unique mono-water structure locked by each B-O-H ternary ring. In addition, the BE of $B_{12}(OH)_{12}^{2-}\cdot nH_2O$ is n times that of mono hydrated per-hydroxylated closo-dodecaborate.

To obtain additional insight into the influence of attraction terms, the total attraction terms were decomposed to three parts: electrostatic (Elst.), induction (Ind.) and dispersion (Disp.) terms. These calculations were performed at the SAPT2+/aug-cc-pVDZ level (Fig. 3c). For all these three hydrates, the electrostatic term dominates the total attraction terms, contributing approximately 62% to the total, while the remaining 38% is attributed to the induction and dispersion terms. This distribution ratio remains invariant across all three hydrates. This differs from the pattern observed in hydrated $B_{12}F_{12}^{2-}\cdot nH_2O$ and $B_{12}I_{12}^{2-}\cdot nH_2O$, where the polarizability of the compounds plays a role in altering the relative importance of the three terms. In the case of mono-hydroxyl functionalization, the weak advantage in binding energies of $B_{12}H_{11}OH^{2-}\cdot nH_2O$ compared to $B_{12}H_{12}^{2-}\cdot nH_2O$ can be attributed to the electrostatic term. And the contribution of electrostatic term ($E_{Elst.}$) to the difference of the total three attraction terms ($\Delta E_{Elst.+Ind.+Disp.}$) between $B_{12}H_{11}OH^{2-}\cdot nH_2O$ and $B_{12}H_{12}^{2-}\cdot nH_2O$ (n = 1–6) are 61%, 64%, 71%, 75%, 75%, and 72%, respectively. While for that between $B_{12}(OH)_{12}^{2-}\cdot nH_2O$ and $B_{12}H_{12}^{2-}\cdot nH_2O$, the contribution from electrostatic term remains constant at 61%, indicating that the increase of total BE after hydroxyl functionalization is primarily due to the electrostatic term. The three-ring locked water structures in $B_{12}(OH)_{12}^{2-}\cdot nH_2O$ clusters lead to a constant growth rate for each attraction term, with the dispersion term exhibiting the largest growth rate, followed by the induction term.

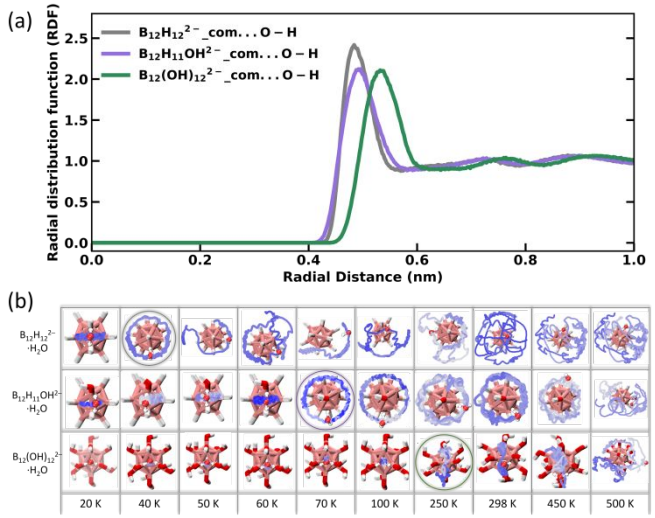

Fig. 4. (a) Radial distribution function (RDF) plots of the distance between centre of mass (com) of $B_{12}H_{12-m}(OH)_m^{2-}$ (m = 0, 1, 12) and O atoms in water shell. (b) Temperature dependent trajectories of water molecules in $B_{12}H_{12-m}(OH)_m^{2-}\cdot H_2O$ (m = 0, 1, 12) during AIMD simulations. Trajectories tracking goes from blue (start) to white (end).

3.4 Aqueous solvation and ab initio molecular dynamics

Inspired by the characteristic hydrated structure growth patterns and the resulting electronic structure evolution, we attempt to describe the influence of hydroxyl groups on the first solvent layer based on force-field molecular dynamics simulations (see details in SI). As shown in Fig. 4(a), the calculated radial distribution function indicates that both $B_{12}H_{12}^{2-}$ and $B_{12}H_{11}OH^{2-}$ exhibit a closer water packing distance compared to $B_{12}(OH)_{12}^{2-}$. The average number of water molecules in the first solvent shell was counted, and it was found that there are approximately 21 water molecules surrounding $B_{12}H_{12}^{2-}$, which is close to the previously reported value of 22.[73] The size of hydrated shell around $B_{12}H_{12}^{2-}$ was enhanced upon mono hydroxyl, resulting in 23 water molecules in the solvation shell of $B_{12}H_{11}OH^{2-}$. $B_{12}(OH)_{12}^{2-}$, characterized by four closed ternary O-H bonds, exhibits largest attached water molecules increasing to 28.

The dynamic properties of water shell also vary with the functional groups. We take the mono hydrated clusters $B_{12}H_{12-m}(OH)_m^{2-}\cdot H_2O$ (m = 0, 1, 12) as a representative to investigate the thermodynamics stability of water molecule controlled by functional groups based on temperature-dependent *ab* initio molecular dynamics (AIMD) analysis (Fig. 4b, see details in SI). As pervious reported, the water molecule moves back and forth around two B-H···H-O dihydrogen bond and is stuck by the B-H bonds on both sides in 20 K for $B_{12}H_{12}^{2-}$.[32] At 40 K, the water molecule begins to move in circular motion along the five B-H vertices, and then enters a random motion around $B_{12}H_{12}^{2-}$ at 50 K. Similarly, in the case of $B_{12}H_{11}OH^{2-}$, the water molecule also undergoes circular motion, but the transition temperature for this motion mode is different. Circular motion occurs at 70 K, and at 500 K, the water molecule exhibits free motion due to the presence of H-O···H-O hydrogen bonds. Notably, when the water moves in a circular motion, the O-H bond of B-O-H group also exhibit clockwork-like motion. In contrast, the addition of hydroxyl functional groups in $B_{12}(OH)_{12}^{2-}$ leads to stronger stabilization of the water shell. At 250 K, the water molecule begins to move within the four B-O-H vertices, indicating confinement to a smaller area compared to $B_{12}H_{12}^{2-}$ and $B_{12}H_{11}OH^{2-}$. At 500 K, the water molecule exhibits free motion, similar to $B_{12}H_{11}OH^{2-}$. Moreover, the movement trajectories observed at 20 K can be correlated with the low-frequency vibration patterns in the simulated infrared spectrum. It is worth noting that there is no significant contribution from the H_2O vibration mode in the infrared spectrum of $B_{12}(OH)_{12}^{2-}\cdot H_2O$, which corresponds to the absence of motion of the water molecule at this temperature. Overall, the introduction of hydroxyl functional groups increases the thermodynamic stability of the water shell and leads to distinct dynamic properties compared to the $B_{12}H_{12}^{2-}$ cluster.

4. Conclusions

In summary, our study provides insights into the reaction mechanism of B-H hydroxylation in $B_{12}H_{12}^{2-}$ using protonated water and hydrogen peroxide as reactants. The reaction energy barriers for these processes are determined to be 8.7 and 31.5 kcal/mol,

respectively. The per-hydroxylated closo-dodecaborate (C_3) retain the globular skeleton of dodecaborate while introducing intra-hydrogen bond network of O-H ternary ring hold by polyhedral core. The hydrated clusters, represented by $B_{12}H_{11}OH^{2-}$ and $B_{12}(OH)_{12}^{2-}$, serve as models to explore the water orientation and the number of the first hydrated shell around the mono- and per-hydroxylated closo-dodecaborates. This allows us to elucidate the molecular-level mechanisms underlying hydroxyl modification and the arrangement of water clusters. In $B_{12}H_{11}OH^{2-}$, the mono B-O-H functional group exhibits unique water distribution characteristics in its immediate vicinity and inherited the arrangement of hydroxide ion (OH^-) within $3H_2O$. For n > 3, the evolution of water clusters are reconciled by intermolecular interaction, including conventional HB B-(H-O)···H-O, DHB B-H···H-O, and inter-water HB O-H···O. In the case of $B_{12}(OH)_{12}^{2-}$, the structure is dominated by the aromatic icosahedral cluster with 4 identical O-H···O ternary rings that lock the water molecules in a fully enclosed form. This structure persists until six water molecules are present, at which point each B-O-H vertex is exhausted, resulting in a C_2 symmetry. The unique structure of the water shell can be attributed to the strong weak interaction energy modified by hydroxyl vertices with more excess negative charge. $B_{12}(OH)_{12}^{2-}$ exhibits dense water clusters with improved thermodynamic stability in the first hydrated shell, resulting in well electrochemical and photochemical behaviours. These findings make it a promising candidate for applications in hydrogen storage and battery technologies, providing a prototype for the development of effective synthetic boron-richer materials.

Author Contributions

Y. J.: methodology, validation, formal analysis, investigation, writing-original draft. Z.H., C. Z. and Y. Y.: formal analysis, investigation. X-B. W. and Z. S.: formal analysis, conceptualization. H. S., Z. L. and P. P.: conceptualization, supervision. All the authors contributed to the discussions.

Conflicts of interest

There are no conflicts to declare.

Acknowledgements

This work is supported by the start-up grant of ShanghaiTech University, Double First-Class Initiative Fund of ShanghaiTech University, Shanghai Rising-Star Program (22QA1406200), National Natural Science Foundation of China (12274297, 92250303), Shanghai Science and Technology Program (21511105000). Part of this research used Beamline 03U of the Shanghai Synchrotron Radiation Facility, which is supported by the ME2 project under contract no. 11227902 from the National Natural Science Foundation of China. ZBH is supported by National Natural Science Foundation of China (12204172). XBW is supported by U.S. Department of Energy (DOE), Office of Science, Office of Basic Energy Sciences, Division of Chemical Science, Geosciences, and Biosciences, Condensed Phase and Interfacial Molecular Science program, FWP 16248.

References

1 G. Giubertoni, O. O. Sofronov and H. J. Bakker, *Commun. Chem.*, 2020, **3**, 84.
2 W. Cai, D. Xu, F. Zhang, J. Wei, S. Lu, L. Qian, Z. Lu and S. Cui, *Nano Res.*, 2022, **15**, 1517-1523.
3 G. Caron, J. Kihlberg and G. Ermondi, *Med. Res. Rev.*, 2019, **39**, 1707-1729.
4 J. R. R. Verlet, A. E. Bragg, A. Kammrath, O. Cheshnovsky and D. M. Neumark, *Science*, 2005, **307**, 93-96.
5 F. F. Jian, E. Liu and J. Y. Ma, *CrystEngComm*, 2018, **20**, 3849-3857.
6 M. Valiev, S. H. M. Deng and X.-B. Wang, *J. Phys. Chem. B*, 2016, **120**, 1518-1525.
7 G. A. Cooper, C. J. Clarke and J. R. R. Verlet, *J. Am. Chem. Soc.*, 2023, **145**, 1319-1326.
8 B. V. Henderson and K. D. Jordan, *J. Phys. Chem. A*, 2019, **123**, 7042-7050.
9 H. K. Gerardi, A. F. DeBlase, X. Su, K. D. Jordan, A. B. McCoy and M. A. Johnson, *J. Phys. Chem. Lett.*, 2011, **2**, 2437-2441.
10 M. Takahashi, N. Ito, N. Haruta, H. Ninagawa, K. Yazaki, Y. Sei, T. Sato and M. Obata, *Commun. Chem.*, 2021, **4**, 168.
11 S. Mirzaei, V. M. Espinoza Castro and R. Hernández Sánchez, *Chem. Sci.*, 2022, **13**, 2026-2032.
12 A. V. Jentzsch, D. Emery, J. Mareda, S. K. Nayak, P. Metrangolo, G. Resnati, N. Sakai and S. Matile, *Nat. Commun.*, 2012, **3**, 905.
13 Y. Tong, I. Y. Zhang and R. K. Campen, *Nat. Commun.*, 2018, **9**, 1313.
14 S. Chen, D. Ji, Q. Chen, J. Ma, S. Hou and J. Zhang, *Nat. Commun.*, 2023, **14**, 3526.
15 S. Ghosal, J. C. Hemminger, H. Bluhm, B. S. Mun, E. L. D. Hebenstreit, G. Ketteler, D. F. Ogletree, F. G. Requejo and M. Salmeron, *Science*, 2005, **307**, 563-566.
16 C. J. C. Jordan, E. A. Lowe and J. R. R. Verlet, *J. Am. Chem. Soc.*, 2022, **144**, 14012-14015.
17 J. K. Denton, P. J. Kelleher, M. A. Johnson, M. D. Baer, S. M. Kathmann, C. J. Mundy, B. A. Wellen Rudd, H. C. Allen, T. H. Choi and K. D. Jordan, *Proc. Natl. Acad. Sci.*, 2019, **116**, 14874-14880.
18 A. Lietard, G. Mensa-Bonsu and J. R. R. Verlet, *Nat. Chem.*, 2021, **13**, 737-742.
19 K. A. Archer and K. D. Jordan, *Chem. Phys. Lett.*, 2016, **661**, 196-199.
20 A. Mukhopadhyay, Y. Yang, Y. Li, Y. Chen, H. Li, A. Natan, Y. Liu, D. Cao and H. Zhu, *Adv. Funct. Mater.*, 2019, **29**, 1903192.
21 X.-Q. Zhang, X. Chen, L.-P. Hou, B.-Q. Li, X.-B. Cheng, J.-Q. Huang and Q. Zhang, *ACS Energy Lett.*, 2019, **4**, 411-416.
22 X. Yang, X.-B. Wang and L.-S. Wang, *J. Phys. Chem. A*, 2002, **106**, 7607-7616.
23 H. Wen, G.-L. Hou, S. M. Kathmann, M. Valiev and X.-B. Wang, *J. Chem. Phys.*, 2013, **138**, 031101.
24 S. S. Xantheas and T. H. Dunning, Jr., *J. Phys. Chem.*, 1994, **98**, 13489-13497.
25 X.-B. Wang, X. Yang, J. B. Nicholas and L.-S. Wang, *Science*, 2001, **294**, 1322-1325.
26 O. Gorlova, J. W. DePalma, C. T. Wolke, A. Brathwaite, T. T. Odbadrakh, K. D. Jordan, A. B. McCoy and M. A. Johnson, *J. Chem. Phys.*, 2016, **145**, 134304.
27 Z. Jing, Y. Zhou, T. Yamaguchi, K. Yoshida, K. Ikeda, K. Ohara and G. Wang, *J. Phys. Chem. Lett.*, 2023, **14**, 6270-6277.
28 W. H. Robertson, E. G. Diken, E. A. Price, J.-W. Shin and M. A. Johnson, *Science*, 2003, **299**, 1367-1372.

29 R. B. King, *Chem. Rev.*, 2001, **101**, 1119-1152.
30 J. Aihara, *J. Am. Chem. Soc.*, 1978, **100**, 3339-3342.
31 E. Aprà, J. Warneke, S. S. Xantheas and X.-B. Wang, *J. Chem. Phys.*, 2019, **150**, 164306.
32 Y. Jiang, Q. Yuan, W. Cao, Z. Hu, Y. Yang, C. Zhong, T. Yang, H. Sun, X.-B. Wang and Z. Sun, *Chem. Sci.*, 2022, **13**, 9855-9860.
33 M. P. Brown and R. W. Heseltine, *Chem. Comm. (London)*, 1968, 1551-1552.
34 A. R. Pitochelli and F. Hawthorne, *J. Am. Chem. Soc.*, 1960, **82**, 3228-3229.
35 Z. Huang, J. Gallucci, X. Chen, T. Yisgedu, H. K. Lingam, S. G. Shore and J.-C. Zhao, *J. Mater. Chem.*, 2010, **20**, 2743-2745.
36 F. Issa, M. Kassiou and L. M. Rendina, *Chem. Rev.*, 2011, **111**, 5701-5722.
37 P. Cígler, M. Kožíšek, P. Řezáčová, J. Brynda, Z. Otwinowski, J. Pokorná, J. Plešek, B. Grüner, L. Dolečková-Marešová, M. Máša, J. Sedláček, J. Bodem, H.-G. Kräusslich, V. Král and J. Konvalinka, *Proc. Natl. Acad. Sci.*, 2005, **102**, 15394-15399.
38 P. Řezáčová, J. Pokorná, J. Brynda, M. Kožíšek, P. Cígler, M. Lepšík, J. Fanfrlík, J. Řezáč, K. Grantz Šašková, I. Sieglová, J. Plešek, V. Šícha, B. Grüner, H. Oberwinkler, J. Sedláček', H.-G. Kräusslich, P. Hobza, V. Král and J. Konvalinka, *J. Med. Chem.*, 2009, **52**, 7132-7141.
39 Y. Jiang, Z. Cai, Q. Yuan, W. Cao, Z. Hu, H. Sun, X.-B. Wang and Z. Sun, *J. Phys. Chem. Lett.*, 2022, **13**, 11787-11794.
40 T. Peymann, C. B. Knobler and M. F. Hawthorne, *Inorg. Chem.*, 2000, **39**, 1163-1170.
41 C. Jenne and C. Kirsch, *Dalton Trans.*, 2015, **44**, 13119-13124.
42 T. Peymann, A. Herzog, C. B. Knobler and M. F. Hawthorne, *Angew. Chem. Int. Ed.*, 1999, **38**, 1061-1064.
43 T. Peymann, C. B. Knobler, S. I. Khan and M. F. Hawthorne, *J. Am. Chem. Soc.*, 2001, **123**, 2182-2185.
44 M. J. Bayer and M. F. Hawthorne, *Inorg. Chem.*, 2004, **43**, 2018-2020.
45 D. Jung, L. M. A. Saleh, Z. J. Berkson, M. F. El-Kady, J. Y. Hwang, N. Mohamed, A. I. Wixtrom, E. Titarenko, Y. Shao, K. McCarthy, J. Guo, I. B. Martini, S. Kraemer, E. C. Wegener, P. Saint-Cricq, B. Ruehle, R. R. Langeslay, M. Delferro, J. L. Brosmer, C. H. Hendon, M. Gallagher-Jones, J. Rodriguez, K. W. Chapman, J. T. Miller, X. Duan, R. B. Kaner, J. I. Zink, B. F. Chmelka and A. M. Spokoyny, *Nat. Mater.*, 2018, **17**, 341-348.
46 M. Jørgensen, S. R. H. Jensen, T. D. Humphries, M. R. Rowles, M. V. Sofianos, C. E. Buckley, T. R. Jensen and M. Paskevicius, *J. Phys. Chem. C*, 2020, **124**, 11340-11349.
47 A. D. Ready, S. M. Becwar, D. Jung, A. Kallistova, E. Schueller, K. P. Anderson, R. Kubena, R. Seshadri, B. F. Chmelka and A. M. Spokoyny, *Dalton Trans.*, 2022, **51**, 11547-11557.
48 L. N. Goswami, L. Ma, S. Chakravarty, Q. Cai, S. S. Jalisatgi and M. F. Hawthorne, *Inorg. Chem.*, 2013, **52**, 1694-1700.
49 E. G. Hohenstein and C. D. Sherrill, *J. Chem. Phys.*, 2010, **133**, 014101.
50 T. M. Parker, L. A. Burns, R. M. Parrish, A. G. Ryno and C. D. Sherrill, *J. Chem. Phys.*, 2014, **140**, 094106.
51 T. Lu, *Molclus Program*, Beijing Kein Research Center for Natural Science: 2016.
52 M. Bursch, H. Neugebauer and S. Grimme, *Angew. Chem. Int. Ed.*, 2019, **58**, 11078-11087.
53 C. Bannwarth, S. Ehlert and S. Grimme, *J. Chem. Theory Comput.*, 2019, **15**, 1652-1671.
54 F. Neese, *Wires Comput. Mol. Sci.*, 2022, **12**, e1606.
55 S. Grimme, J. Antony, S. Ehrlich and H. Krieg, *J. Chem. Phys.*, 2010, **132**, 154104.
56 S. Grimme, S. Ehrlich and L. Goerigk, *J. Comput. Chem.*, 2011, **32**, 1456-1465.
57 R. A. Kendall, T. H. Dunning and R. J. Harrison, *J. Chem. Phys.*, 1992, **96**, 6796-6806.
58 K. A. Peterson, B. C. Shepler, D. Figgen and H. Stoll, *J. Phys. Chem. A*, 2006, **110**, 13877-13883.
59 C. Riplinger, B. Sandhoefer, A. Hansen and F. Neese, *J. Chem. Phys.*, 2013, **139**, 134101.
60 F. Neese, F. Wennmohs and A. Hansen, *J. Chem. Phys.*, 2009, **130**, 114108.
61 J. P. Merrick, D. Moran and L. Radom, *J. Phys. Chem. A*, 2007, **111 45**, 11683-11700.
62 A. K. Dutta, M. Saitow, C. Riplinger, F. Neese and R. Izsák, *J. Chem. Phys.*, 2018, **148**, 244101.
63 R. M. Parrish, L. A. Burns, D. G. A. Smith, A. C. Simmonett, A. E. DePrince, E. G. Hohenstein, U. Bozkaya, A. Y. Sokolov, R. Di Remigio, R. M. Richard, J. F. Gonthier, A. M. James, H. R. McAlexander, A. Kumar, M. Saitow, X. Wang, B. P. Pritchard, P. Verma, H. F. Schaefer, K. Patkowski, R. A. King, E. F. Valeev, F. A. Evangelista, J. M. Turney, T. D. Crawford and C. D. Sherrill, *J. Chem. Theory Comput.*, 2017, **13**, 3185-3197.
64 T. Lu and F. Chen, *J. Comput. Chem.*, 2012, **33**, 580-592.
65 W. Humphrey, A. Dalke and K. Schulten, *J. Mol. Graph. Model.*, 1996, **14**, 33-38.
66 M. J. Frisch, G. W. Trucks, H. B. Schlegel, G. E. Scuseria, M. A. Robb, J. R. Cheeseman, G. Scalmani, V. Barone, G. A. Petersson, H. Nakatsuji, X. Li, M. Caricato, A. V. Marenich, J. Bloino, B. G. Janesko, R. Gomperts, B. Mennucci, H. P. Hratchian, J. V. Ortiz, A. F. Izmaylov, J. L. Sonnenberg, Williams, F. Ding, F. Lipparini, F. Egidi, J. Goings, B. Peng, A. Petrone, T. Henderson, D. Ranasinghe, V. G. Zakrzewski, J. Gao, N. Rega, G. Zheng, W. Liang, M. Hada, M. Ehara, K. Toyota, R. Fukuda, J. Hasegawa, M. Ishida, T. Nakajima, Y. Honda, O. Kitao, H. Nakai, T. Vreven, K. Throssell, J. A. Montgomery Jr., J. E. Peralta, F. Ogliaro, M. J. Bearpark, J. J. Heyd, E. N. Brothers, K. N. Kudin, V. N. Staroverov, T. A. Keith, R. Kobayashi, J. Normand, K. Raghavachari, A. P. Rendell, J. C. Burant, S. S. Iyengar, J. Tomasi, M. Cossi, J. M. Millam, M. Klene, C. Adamo, R. Cammi, J. W. Ochterski, R. L. Martin, K. Morokuma, O. Farkas, J. B. Foresman and D. J. Fox, *Gaussian 16 Rev. A.03*, Wallingford, CT, 2016.
67 M. J. Abraham, T. Murtola, R. Schulz, S. Páll, J. C. Smith, B. Hess and E. Lindahl, *SoftwareX*, 2015, **1-2**, 19-25.
68 X.-Z. Li, B. Walker and A. Michaelides, *Proc. Natl. Acad. Sci.*, 2011, **108**, 6369-6373.
69 W. Cao, H. Wen, S. S. Xantheas and X.-B. Wang, *Sci. Adv.*, 2023, **9**, eadf4309.
70 B. Zhang, Y. Yu, Y.-Y. Zhang, S. Jiang, Q. Li, H.-S. Hu, G. Li, Z. Zhao, C. Wang, H. Xie, W. Zhang, D. Dai, G. Wu, H. Zhang Dong, L. Jiang, J. Li and X. Yang, *Proc. Natl. Acad. Sci.*, 2020, **117**, 15423-15428.
71 J. Warneke, G.-L. Hou, E. Aprà, C. Jenne, Z. Yang, Z. Qin, K. Kowalski, X.-B. Wang and S. S. Xantheas, *J. Am. Chem. Soc.*, 2017, **139**, 14749-14756.
72 Y. Jiang, Q. Yuan, W. Cao, M. Rohdenburg, M. C. Nierstenhöfer, Z. Li, Y. Yang, C. Zhong, C. Jenne, J. Warneke, H. Sun, Z. Sun and X.-B. Wang, *Phys. Chem. Chem. Phys.*, 2021, **23**, 13447-13457.
73 K. Karki, D. Gabel and D. Roccatano, *Inorg. Chem.*, 2012, **51**, 4894-4896.